Journal of Sound and Vibration 326 (2009) 753–767

Contents lists available at ScienceDirect

Journal of Sound and Vibration

journal homepage: www.elsevier.com/locate/jsvi

A component mode synthesis algorithm for multibody dynamics of wind turbines

K. Holm-Jørgensen *, S.R.K. Nielsen [1]

Department of Civil Engineering, Aalborg University, Sohngaardsholmsvej 57, DK-9000 Aalborg, Denmark

ARTICLE INFO

Article history:
Received 29 September 2008
Received in revised form
4 May 2009
Accepted 6 May 2009
Handling Editor: M.P. Cartmell
Available online 5 June 2009

ABSTRACT

A system reduction scheme related to a multibody formulation of wind turbine dynamics is devised. Each substructure is described in its own frame of reference, which is moving freely in the vicinity of the moving substructure, in principle without any constraints to the rigid body part of the motion of the substructure. The system reduction is based on a component mode synthesis method, where the response of the internal degrees of freedom of the substructure is described as the quasi-static response induced by the boundary degrees of freedom via the constraint modes superimposed in combination to a dynamic component induced by inertial effects and internal loads. The latter component is modelled by a truncated modal expansion in fixed interface undamped eigenmodes. The selected modal vector base for the internal dynamics ensures that the boundary degrees of freedom account for the rigid-body dynamics of the substructure, and explicitly represent the coupling degrees of freedom at the interface to the adjacent substructures. The method has been demonstrated for a blade structure, which has been modelled as two substructures. Two modelling methods have been examined where the first is by use of fixed–fixed eigenmodes for the innermost substructure and fixed–free eigenmodes for the outermost substructure. The other approach is by use of fixed–free eigenmodes for both substructures. The fixed–fixed method shows good correspondence with the full FE model which is not the case for the fixed–free method due to incompatible displacements and rotations at the interface between the two substructures. Moreover, the results from the reduced model by use of constant constraint modes and constant fixed interface modes over a large operating area for the wind turbine blade are almost identical to the full FE model.

1. Introduction

Flexible multibody based simulations of the dynamic behaviour of a wind turbine requires a discretization in space for each substructure of the system. Typically, this is done by an FE method, often involving many degrees of freedom for each substructure. In order to reduce the computational effort, reduced order models of the substructures need to be implemented. Especially, this is necessary in stochastic analyses based on Monte Carlo simulations, or during the design phase of a wind turbine, where multiple load cases need to be analysed. A reduced order model is also necessary in some active vibration control algorithms, where the structural model must be processed in real time. Due to the geometric

* Corresponding author.
E-mail addresses: khj@civil.aau.dk (K. Holm-Jørgensen), soren.nielsen@civil.aau.dk (S.R.K. Nielsen).
[1] Tel.: +45 99 40 84 51; fax: +45 98 14 25 55.

0022-460X/$ - see front matter © 2009 Elsevier Ltd. All rights reserved.
doi:10.1016/j.jsv.2009.05.007

complexity of the blades, which otherwise requires many elements to model, the system reduction in this paper is focused on the blades.

The basic idea of flexible multibody dynamics is to introduce a moving frame of reference to each substructure. Relative to the moving frame elastic displacements are relatively small, rendering linear analysis possible. Hence, nonlinearities are confined to the description of the moving frame. This is defined by a position vector and a parameter vector, also known as a pseudovector, defining the origin and rotation of the moving frame relative to a fixed frame of reference. The standard formulation of multibody methods requires that there is no rigid-body motion between the substructure and its moving frame. In Agrawal and Shabana [1] an automated method is derived to eliminate the rigid-body motion of the body relative to the moving frame. This is done by imposing reference conditions by use of a boolean matrix on the shape functions whereby the deformation modes become consistent with the boundary conditions. In Shabana [2] it is demonstrated that two sets of deformation modes associated with two different sets of boundary conditions e.g. simply supported and free–free can be used to obtain the same solution provided that the moving frame is properly selected. The position and orientation of the moving frame is defined by a set of Lagrangian coordinates that describe the rigid-body translation and rotation. Hereby, these coordinates become a part of the degrees of freedom of the multibody system, see e.g. Nikravesh [3], García and Bayo [4], Géradin and Cardona [5] and Shabana [6]. The use of such a mixed set of referential and elastic coordinates leads to highly nonlinear system equations. Further, as a result of the inertial coupling between the said degrees of freedom the mass matrix depends on the referential coordinates, even when formulated in the moving frame. To circumvent these difficulties Kawamoto et al. [7–10] suggested to let the moving frame of reference float in a controlled way relative to the moving substructure, so these are always sufficiently close to each other, in order for the small displacement assumption to be fulfilled. Hereby, the system matrices do not depend on the generalized coordinates by explicitly predicting the rigid-body motion. To reduce or eliminate the gap between the predicted and actual motion, it is necessary to regularly update the motion of the moving frame of reference as demonstrated in Kawamoto et al. [10]. The main difference to the multibody formulation described in Agrawal and Shabana [1] and Shabana [2] is that the parameters for the moving frame do not enter as degrees of freedom in the system state vector and that it is possible for the body to have a small rigid-body displacement relative to the moving frame. In Kawamoto et al. [7] the updating scheme is originally described, where the orientation, angular velocity, and angular acceleration of the moving frame are updated based on a local triad linked to four nodes in the body. In Kawamoto et al. [8] the local triad is updated based on a polar decomposition. In Kawamoto et al. [9,10] rigid-body modes are used to update the motion of the moving frame. In a previous paper by the present authors [11] the same approach as described in Kawamoto et al. [8] by using a freely moving frame in a multibody formulation is adopted. Here, the wind turbine blade is modelled by only one multibody and reduced by a Ritz bases consisting of rigid-body and elastic fixed-base eigenmodes. Moreover, the quasi-static contribution from the truncated elastic modes is included in the formulation. In order to get a better description of the large nonlinear displacements of a wind turbine blade it is necessary to include more than one multibody in the blade. The purpose of the present paper is to demonstrate a general approach for including an arbitrary number of reduced multibodies to model e.g. a wind turbine blade. The updating scheme of the moving frame of reference in the present paper follows the same principles as described in Kawamoto et al. [8]. A small change when updating the moving frame is presented, where the orientation of the moving frame is updated based on the motion of two boundary nodes. It is possible to use other nodes than the boundary nodes in the updating procedure. The selected updating nodes may even be shifted during a numerical simulation, if this is considered favourable in reducing the displacements of the substructure relative to the moving frame. It should be noticed that possible geometrical nonlinear elastic deformations may be further reduced or removed by subdividing the considered substructure.

The following outline presumes a partitioning of the degrees of freedom of the substructure in the boundary degrees at the interface to the adjacent substructures and the remaining interior degrees of freedom. Static condensation proposed by Guyan [12] completely ignores dynamics of the interior degrees of freedom, which are described as a linear function of the boundary degrees of freedom. Hence, the substructure is completely described by the boundary degrees of freedom. It is well-known that this method in principle is a Ritz method, and hence leads to an overestimation of the natural frequencies, see e.g. Bathe [13]. The so-called dynamic condensation method, proposed by Leung [14–16], Petersmann [17] and others, is an extension of the static condensation method in the sense that a few boundary degrees of freedom are kept and the remaining interior degrees of freedom are eliminated in terms of these. Contrary to static condensation, the condensation matrix contains inertial and damping terms for the interior degrees of freedom and thereby time derivatives of these, which make iterations necessary. Often the Guyan reduction is used in the first iteration. Variants of the iterative methods have been given in [18–21]. In the present paper no iterations are performed in the condensation matrix. The method resembles the specific realization of the component mode synthesis (CMS) method known as the constraint-mode method, which consists of rigid-body modes, constraint modes and fixed interface normal modes to describe the interior dynamics, Hurty [22,23]. Constraint modes are defined as static deformation modes, where the substructure is free of internal loads, and where each boundary degree of freedom in turn is given a unit displacement with the remaining boundary degrees of freedom fixed. Hence, these modes represent the modes available in static condensation. The fixed interface normal modes representing the interior dynamics are determined from the generalized eigenvalue problem of the internal degrees of freedom. Craig and Bampton [24] simplified the approach considerable by treating rigid-body modes as a special case of constraint modes. The method in the present paper is based on this Craig–Bampton method.

Ambrósio and Gonçalves [25] used a traditional multibody formulation with a mixed set of reference and elastic coordinates. The elastic coordinates were later described by a reduced number of fixed interface modal coordinates. Shanmugan and Padmanabhan [26] have described a hybrid fixed–free CMS method for rotordynamic analysis which showed better accuracy than the traditional fixed–fixed and free–free methods. The reason for this is that the boundary displacements in this case represent the exact coupling degrees of freedom, unaffected by the interior dynamics. This compatibility is also achieved by the method in the present paper, and its importance is demonstrated by modelling the blade by two substructures both by use of fixed–free eigenmodes. Hereby, compatibility at the assembling point between the two substructures is not fulfilled, except for a large number of included eigenmodes. Moreover, the purpose in this paper is to demonstrate that constant constraint modes and constant fixed interface normal modes can be used over a wide operating area, where the wind turbine blade speeds up from a stopped situation to its nominal operating situation.

2. Moving frame of reference formulation of multibody dynamics

The idea is to describe the motion of a substructure in a (x_1,x_2,x_3)-coordinate system, which is freely moving in the vicinity of the substructure. Further, a fixed $(\bar{x}_1,\bar{x}_2,\bar{x}_3)$-coordinate system is introduced common for all substructures. Accordingly, fixed frame and moving frame components of vectors and tensors will be indicated with and without a bar, respectively. The origin of the moving coordinate system is described by a position vector with the global components $\bar{\mathbf{x}}_c$, and its rotation is determined by the parameter vector (or pseudovector) $\boldsymbol{\theta}$. The angular velocity and angular acceleration vectors of the moving frame are specified by their moving frame components $\boldsymbol{\omega}$ and $\boldsymbol{\alpha}$, respectively. Generally, the substructure may drift away from the moving frame, which requires sequential updating of the position, velocity and acceleration of the origin together with the rotation, angular velocity and angular acceleration vectors to ensure small displacement components of the substructure relative to the moving frame, but also for the gyroscopic loads on the substructure to be determined with a satisfying accuracy. The essential point is that the degrees of freedom for the substructure and the parameters defining the moving frame are independently specified. Therefore, it is possible to have rigid-body displacements of the body relative to the moving frame. This gap should be sufficiently small in order for the small displacement assumption to be fulfilled. The gap can be reduced or eliminated by updating the motion of the moving frame iteratively. At time $t=t_j$ the position of a substructure and its belonging moving frame of reference are illustrated in Fig. 1a. $\mathbf{s}$ is a position vector along the moving x_3-axis, identifying a given cross-section of the beam, and $\mathbf{u}(\mathbf{s},t)$ is the moving coordinates of the displacement field for the centroid of the cross-section. $\mathbf{u}(\mathbf{s},t)$ is determined by shape functions in the FE model and mode shapes in the reduced model, both with corresponding generalized coordinates $\mathbf{y}(t)$ and $\mathbf{w}(t)$, respectively. Figs. 1b and c display various possibilities for updating theposition of the moving frame of reference relative to the moving beam-like substructure at the time $t_{j+1}=t_j+\Delta t$ where Δt denotes the elapsed time step. Figs. 1b and c show the cases, where the motion at one and two boundary nodes, respectively, will be used to update the parameters for the moving frame. The latter will in most cases reduce the displacements of the substructure from the moving frame compared to only using one boundary node in the update. Because the moving frame of reference parameters enter the equations of motion it is necessary to iteratively update these parameters together with the motion of the substructure, which will be described in a later section.

First, the equations of motion for a constrained multibody system are described. The position vector to a material point within the substructure has the following moving and fixed frame components:

$$\mathbf{x}(\mathbf{s},t)=\mathbf{s}+\mathbf{u}(\mathbf{s},t) \tag{1}$$

$$\bar{\mathbf{x}}(\mathbf{s},t)=\bar{\mathbf{x}}_c+\mathbf{R}(\mathbf{s}+\mathbf{u}(\mathbf{s},t)) \tag{2}$$

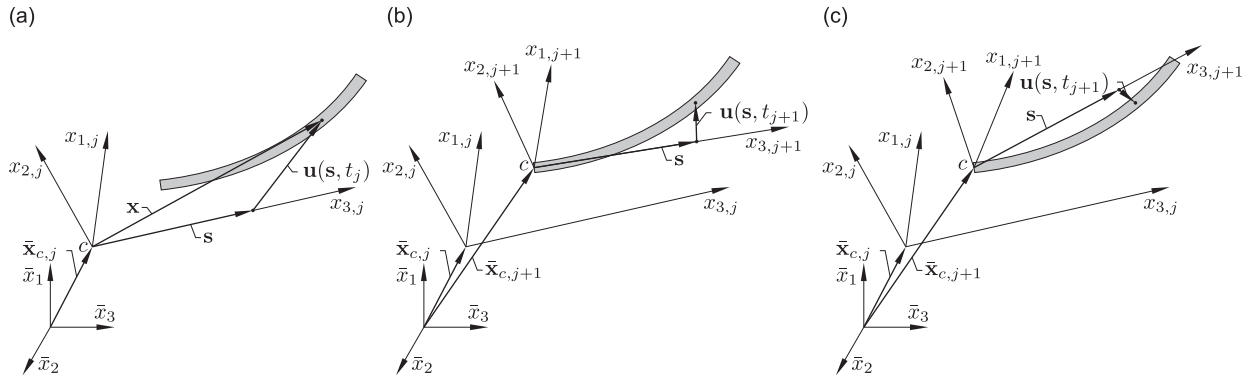

Fig. 1. (a) A substructure and the belonging moving frame of reference at time $t=t_j$. At time $t_{j+1}=t_j+\Delta t$ the moving frame of reference has been updated based on: (b) the motion of one boundary node; (c) the motion of both boundary nodes.

where $\mathbf{R}$ stores the components of the rotation tensor related to the moving frame. $\mathbf{R}$ is defined by the pseudovector $\boldsymbol{\theta}$ as given by the Rodriquez formula, see e.g. Shabana [6]

$$\mathbf{R} = \cos\theta\mathbf{I} + (1-\cos\theta)\mathbf{n}\mathbf{n}^{\mathrm{T}} + \sin\theta\tilde{\mathbf{n}} \tag{3}$$

where $\mathbf{n} = \boldsymbol{\theta}/|\boldsymbol{\theta}|$ is the rotation unit vector. $\mathbf{n}\mathbf{n}^{\mathrm{T}}$ is the outer product of this vector with itself, and $\tilde{\mathbf{n}}$ is the spin matrix related to $\mathbf{n}$. $\tilde{\mathbf{n}}$ is given as

$$\tilde{\mathbf{n}} = \begin{bmatrix} 0 & -n_3 & n_2 \\ n_3 & 0 & -n_1 \\ -n_2 & n_1 & 0 \end{bmatrix} \tag{4}$$

$[n_1, n_2, n_3]$ specify the components of $\mathbf{n}$. These are the same in the fixed and the moving coordinate systems. The corresponding moving frame components of the velocity and acceleration vector of the material point become

$$\mathbf{v} = \mathbf{v}_c + \tilde{\boldsymbol{\omega}}(\mathbf{s}+\mathbf{u}) + \dot{\mathbf{u}} \tag{5}$$

$$\mathbf{a} = \mathbf{a}_c + (\tilde{\boldsymbol{\alpha}} + \tilde{\boldsymbol{\omega}}\tilde{\boldsymbol{\omega}})(\mathbf{s}+\mathbf{u}) + 2\tilde{\boldsymbol{\omega}}\dot{\mathbf{u}} + \ddot{\mathbf{u}} \tag{6}$$

where $\boldsymbol{\alpha} = \dot{\boldsymbol{\omega}}$. $\tilde{\boldsymbol{\omega}}$ and $\tilde{\boldsymbol{\alpha}}$ denote the spin matrices in moving coordinates related to $\boldsymbol{\omega}$ and $\boldsymbol{\alpha}$. The first term $\mathbf{v}_c$ in Eq. (5) is the translational velocity of the moving frame, the second term $\tilde{\boldsymbol{\omega}}(\mathbf{s}+\mathbf{u})$ is the rotational velocity, and the last term $\dot{\mathbf{u}}$ stores the moving coordinates of the velocity from elastic deformations and rigid-body motions inside the moving frame. The first term $\mathbf{a}_c$ in Eq. (6) denotes the translational acceleration of the moving frame origin. The term $\tilde{\boldsymbol{\alpha}}(\mathbf{s}+\mathbf{u})$ is the angular acceleration which is orthogonal on $\boldsymbol{\alpha}$ and $(\mathbf{s}+\mathbf{u})$. The next term $\tilde{\boldsymbol{\omega}}\tilde{\boldsymbol{\omega}}(\mathbf{s}+\mathbf{u}) = \boldsymbol{\omega}\times(\boldsymbol{\omega}\times(\mathbf{s}+\mathbf{u}))$ describes the centrifugal acceleration. The Coriolis acceleration in moving coordinates is described by $2\tilde{\boldsymbol{\omega}}\dot{\mathbf{u}}$ which is perpendicular to both the direction of the velocity of the moving body and to the rotation axis. Finally, the term $\ddot{\mathbf{u}}$ describes the moving frame components of the acceleration of the material point as seen by an observer in the moving frame. Based on an FE discretization the local displacement field for a beam element is interpolated in the form

$$\begin{aligned} &\mathbf{u}_{\mathrm{el}}(\mathbf{s}_{\mathrm{el}}, t) = \mathbf{N}_{\mathrm{el}}(\mathbf{s}_{\mathrm{el}})\mathbf{y}_{\mathrm{el}}(t) \\ &\mathbf{N}_{\mathrm{el}}(\mathbf{s}_{\mathrm{el}}) = \begin{bmatrix} N_2 & 0 & 0 & 0 & N_3 & 0 & N_5 & 0 & 0 & 0 & N_6 & 0 \\ 0 & N_2 & 0 & -N_3 & 0 & 0 & 0 & N_5 & 0 & -N_6 & 0 & 0 \\ 0 & 0 & N_1 & 0 & 0 & 0 & 0 & 0 & N_4 & 0 & 0 & 0 \end{bmatrix} \\ &N_1 = 1-\xi, \quad N_2 = 2\xi^3 - 3\xi^2 + 1, \quad N_3 = (\xi^3 - 2\xi^2 + \xi)L_{\mathrm{el}} \\ &N_4 = \xi, \quad N_5 = -2\xi^3 + 3\xi^2, \quad N_6 = (\xi^3 - \xi^2)L_{\mathrm{el}} \end{aligned} \tag{7}$$

$\xi = s_{\mathrm{el}}/L_{\mathrm{el}}$ is a dimensionless interpolation parameter where s_{el} is a local reference length from the beginning $s_{\mathrm{el}} = 0$ to the end $s_{\mathrm{el}} = L_{\mathrm{el}}$ of the element and L_{el} is the reference length of the beam element. $\mathbf{y}_i(t)$ is the degrees of freedom of the FE model of the substructure i. In a beam model they represent the moving coordinates of the nodal displacements and rotations relative to the moving frame of reference and $\mathbf{N}_i(\mathbf{s})$ is an interpolation matrix. The equations of motion of the substructure i are conveniently derived using analytical mechanics using an extended Lagrangian to account for the kinematic constraints, in combination with the kinetic energy $T = T(\mathbf{y}_i, \dot{\mathbf{y}}_i)$ and the potential energy $U = U(\mathbf{y}_i)$ from all substructures. The latter contains contributions from the strain energy and conservative external loads $\mathbf{Q}_{c,i}(\mathbf{y}_i)$ such as gravity, in addition to vectorial quantities as the non-conservative loads $\mathbf{Q}_{nc,i}(\mathbf{y}_i)$. In principle, these loads may be linearized in the applied moving frame of reference. The non-conservative loads are caused by the follower character of the aerodynamic loads. The kinetic energy is most convenient determined by use of the moving frame components of the velocity vector $\mathbf{v}$ from Eq. (5). In a slightly modified version of those given by Kawamoto et al. [8] the resulting equations become

$$\begin{aligned} &\mathbf{M}_i\ddot{\mathbf{y}}_i + (\mathbf{C}_{0,i} + 2\mathbf{G}_i)\dot{\mathbf{y}}_i + (\mathbf{K}_{e,i} + \dot{\mathbf{G}}_i + \mathbf{D}_i + \mathbf{K}_{g,i})\mathbf{y}_i + \mathbf{B}_i^{\mathrm{T}}(\mathbf{y}_i)\bar{\boldsymbol{\lambda}}_i \\ &\quad = -\mathbf{M}_{0,i}^{\mathrm{T}}\mathbf{a}_{c,i} - \dot{\mathbf{J}}_{0,i}^{\mathrm{T}} + \mathbf{J}_{2,i}^{\mathrm{T}} + \mathbf{Q}_{c,i}(\mathbf{y}_i) + \mathbf{Q}_{nc,i}(\mathbf{y}_i) \end{aligned} \tag{8}$$

where the Lagrange multipliers $\bar{\boldsymbol{\lambda}}_i$ contain the global components of the reaction forces and moments conjugated to the kinematic constraints and $\mathbf{B}_i^{\mathrm{T}}(\mathbf{y}_i)$ is the constraint matrix. Because the constraints have been formulated in the fixed frame of reference the components of $\bar{\boldsymbol{\lambda}}$ are also in the fixed frame. The symmetric matrices $\mathbf{C}_{0,i}$ and $\mathbf{K}_{e,i}$ denote the structural damping and elastic stiffness matrix, respectively. The latter includes bending, torsional, and axial stiffnesses. $\mathbf{K}_{g,i}$ denotes the geometrical stiffness matrix. For a beam-like substructure of the length L this may be written as

$$\mathbf{K}_{g,i} = \Omega^2(t)\int_L Q_3(x_3, t)\frac{\mathrm{d}\mathbf{N}_{g,i}^{\mathrm{T}}}{\mathrm{d}x_3}\frac{\mathrm{d}\mathbf{N}_{g,i}}{\mathrm{d}x_3}\,\mathrm{d}x_3 \tag{9}$$

where $Q_3(x_3, t)$ represents the distribution of the centrifugal axial force for $\Omega = 1$, so $\Omega^2(t)Q_3(x_3, t)$ denotes the axial force at the position x_3. $\mathbf{N}_{g,i}$ includes the two first rows in $\mathbf{N}_i$ which represent the two displacement components orthogonal to the beam axis. For a wind turbine blade the axial load is caused by the centrifugal and gravity forces. During operation the

geometric stiffness from the centrifugal axial force will assist to stretch out the blade corresponding to an increased stiffness and thereby reduce the displacements in the flap direction. Moreover, this term has shown to increase the stability of the numerical model. The other matrices and vectors are defined as

$$\mathbf{M}_i = \int_L \mathbf{N}_i^{\mathrm{T}} \mathbf{N}_i \mu \, \mathrm{d}x_3, \quad \mathbf{M}_{0,i} = \int_L \mathbf{N}_i \mu \, \mathrm{d}x_3, \quad \mathbf{D}_i = \int_L \mathbf{N}_i^{\mathrm{T}} \tilde{\boldsymbol{\omega}}_i \tilde{\boldsymbol{\omega}}_i \mathbf{N}_i \mu \, \mathrm{d}x_3 \tag{10}$$

$$\mathbf{G}_i = \int_L \mathbf{N}_i^{\mathrm{T}} \tilde{\boldsymbol{\omega}}_i \mathbf{N}_i \mu \, \mathrm{d}x_3, \quad \mathbf{J}_{0,i} = \boldsymbol{\omega}_i^{\mathrm{T}} \int_L \tilde{\mathbf{s}} \mathbf{N}_i \mu \, \mathrm{d}x_3, \quad \mathbf{J}_{2,i} = \boldsymbol{\omega}_i^{\mathrm{T}} \int_L \tilde{\mathbf{s}} \tilde{\boldsymbol{\omega}}_i \mathbf{N}_i \mu \, \mathrm{d}x_3 \tag{11}$$

$$\dot{\mathbf{G}}_i = \int_L \mathbf{N}_i^{\mathrm{T}} \tilde{\boldsymbol{\alpha}}_i \mathbf{N}_i \mu \, \mathrm{d}x_3, \quad \dot{\mathbf{J}}_{0,i} = \boldsymbol{\alpha}_i^{\mathrm{T}} \int_L \tilde{\mathbf{s}} \mathbf{N}_i \mu \, \mathrm{d}x_3 \tag{12}$$

$\mathbf{M}_i$ is the conventional symmetric mass matrix of the body in the moving frame of reference, which in the present formulation is independent of the moving frame of reference parameters. $\mu = \mu(\mathbf{s})$ denotes the mass per unit length. $\mathbf{M}_{0,i}$ is a matrix representing the inertial effect of uniform translation. The effect of centrifugal forces due to elastic deformations is contained in the symmetric matrix $\mathbf{D}_i$ and the gyroscopic forces are represented by the skew symmetric matrix $\mathbf{G}_i$. The remaining $\mathbf{J}_{0,i}$ and $\mathbf{J}_{2,i}$ terms are couplings between the reference position and the shape functions. In Kawamoto et al. [10] it is shown how $\mathbf{D}_i$, $\mathbf{G}_i$, and $\dot{\mathbf{G}}_i$ can be simplified by extracting $\tilde{\boldsymbol{\omega}}_i$ and $\tilde{\boldsymbol{\alpha}}_i$ outside the integration for isoparametric volume elements. For ease the nonlinearity displayed by the dependency of $\mathbf{y}_i$ in the load vector is neglected, whereby the equations of motion conveniently are written in the form

$$\mathbf{M}_i \ddot{\mathbf{y}}_i + \mathbf{C}_i \dot{\mathbf{y}}_i + \mathbf{K}_i \mathbf{y}_i + \mathbf{B}_i^{\mathrm{T}}(\mathbf{y}_i) \bar{\lambda}_i = \mathbf{f}_i(t) \tag{13}$$

where

$$\mathbf{C}_i = \mathbf{C}_{0,i} + 2\mathbf{G}_i, \quad \mathbf{K}_i = \mathbf{K}_{e,i} + \dot{\mathbf{G}}_i + \mathbf{D}_i + \mathbf{K}_{g,i} \tag{14}$$

$$\mathbf{f}_i(t) = -\mathbf{M}_{0,i}^{\mathrm{T}} \mathbf{a}_{c,i} - \dot{\mathbf{J}}_{0,i}^{\mathrm{T}} + \mathbf{J}_{2,i}^{\mathrm{T}} + \mathbf{Q}_{c,i} + \mathbf{Q}_{nc,i} \tag{15}$$

$\mathbf{C}_i$ and $\mathbf{K}_i$ may be interpreted as resulting non-symmetric damping and stiffness matrices for the unconstrained substructure.

To set up the equations of motion for a multibody system it is necessary to introduce kinematical constraints in order to incorporate compatibility of the mutual displacements and rotations of the substructures. In relation to wind turbines, displacement constraints between the rotor shaft and the nacelle are specified at the bearings of the nacelle. Rotational constraints are e.g. prescribed between the rotor shaft and the blade substructure in terms of a controlled pitch angle. The kinematic constraints are vector relations with components, which need to be defined in a common coordinate system e.g. a global fixed coordinate system or the moving frame of reference of one of the substructures. The following constraint equations can be generalized to an arbitrary number of constraints and substructures, but are here shown for two adjacent substructures. Below, $\mathbf{s}_{1,0}$ and $\mathbf{s}_{2,0}$ denote the referential position vectors in the respective moving frames, defining a point in substructures 1 and 2 at which a kinematical displacement constraint is specified, and $\mathbf{u}_{1,0}$ and $\mathbf{u}_{2,0}$ are the corresponding displacement vectors. A displacement constraint which fixes the position of two arbitrary points in the substructures 1 and 2 becomes, cf. Eq. (2)

$$\begin{aligned} \boldsymbol{\Phi}_{\mathrm{dc}} &= \bar{\mathbf{x}}_{c1} + \mathbf{R}_1(\mathbf{s}_{1,0} + \mathbf{u}_{1,0}) - (\bar{\mathbf{x}}_{c2} + \mathbf{R}_2(\mathbf{s}_{2,0} + \mathbf{u}_{2,0})) \\ &= \bar{\mathbf{x}}_{c1} + \mathbf{R}_1(\mathbf{s}_{1,0} + \mathbf{N}_{1,0}\mathbf{y}_1) - (\bar{\mathbf{x}}_{c2} + \mathbf{R}_2(\mathbf{s}_{2,0} + \mathbf{N}_{2,0}\mathbf{y}_2)) \\ &= \mathbf{B}_{d,1}\mathbf{y}_1 - \mathbf{B}_{d,2}\mathbf{y}_2 - \mathbf{b} = \mathbf{0} \end{aligned} \tag{16}$$

$$\mathbf{B}_{d,i} = \mathbf{R}_i \mathbf{N}_{i,0}, \quad \mathbf{b} = -(\bar{\mathbf{x}}_{c1} + \mathbf{R}_1 \mathbf{s}_{1,0}) + (\bar{\mathbf{x}}_{c2} + \mathbf{R}_2 \mathbf{s}_{2,0})$$

In an FE formulation, where $\mathbf{u}_i(\mathbf{s}_i, t)$ is interpolated by a set of shape functions $\mathbf{N}_i(\mathbf{s}_i)$ and degrees of freedom $\mathbf{y}_i(t)$, $\mathbf{u}_{i,0}(t) = \mathbf{N}_{i,0}\mathbf{y}_i(t)$, where $\mathbf{N}_{i,0} = \mathbf{N}_i(\mathbf{s}_{i,0})$. Further, $\mathbf{R}_1$ and $\mathbf{R}_2$ represent the rotation tensors of the moving frames relative to the global coordinate system. Let $\boldsymbol{\varphi}_{i,0}$ denote the local rotation components of the interface node relative to the moving frame of substructure i. The rotation tensor of the said node is then given by

$$\mathbf{R}_i^* = \mathbf{R}_i \mathbf{R}(\boldsymbol{\varphi}_{i,0}) \simeq \mathbf{R}_i(\mathbf{I} + \tilde{\boldsymbol{\varphi}}_{i,0}) \tag{17}$$

where the indicated linearization presumes $|\boldsymbol{\varphi}_{0,i}| \ll 1$. Let $\mathbf{n}_1$ and $\mathbf{n}_2$ be the local components in the moving coordinate systems of unit vectors attached to the interface nodes in substructures 1 and 2. The rotation of these vectors is given as $\mathbf{R}_1^*\mathbf{n}_1$ and $\mathbf{R}_2^*\mathbf{n}_2$, respectively. Assume that the vectors before and during the elastic deformation of the interface nodes remain orthogonal. Then the rotational constraint can be specified as

$$\Phi_{\mathrm{rc}} = (\mathbf{R}_1^*\mathbf{n}_1)^{\mathrm{T}} \mathbf{R}_2^* \mathbf{n}_2 = 0 \tag{18}$$

A total of three scalar products are necessary to fix the rotations in the joint. In the following derivations, focus is on a fixed interface where the unit vectors are orthogonal throughout the simulations. By insertion of Eq. (17) in Eq. (18) the

rotational constraint becomes

$$\begin{aligned}\Phi_{rc} &= \mathbf{n}_2^{\mathrm{T}}\mathbf{R}_2^{\mathrm{T}}\mathbf{R}_1\tilde{\mathbf{n}}_1\boldsymbol{\varphi}_{1,0} + \mathbf{n}_1^{\mathrm{T}}\mathbf{R}_1^{\mathrm{T}}\mathbf{R}_2\tilde{\mathbf{n}}_2\boldsymbol{\varphi}_{2,0} - \mathbf{n}_1^{\mathrm{T}}\mathbf{R}_1^{\mathrm{T}}\mathbf{R}_2\mathbf{n}_2 + \boldsymbol{\varphi}_{1,0}^{\mathrm{T}}\tilde{\mathbf{n}}_1\mathbf{R}_1^{\mathrm{T}}\mathbf{R}_2\tilde{\mathbf{n}}_2\boldsymbol{\varphi}_{2,0}\\ &= \mathbf{n}_2^{\mathrm{T}}\mathbf{R}_2^{\mathrm{T}}\mathbf{R}_1\tilde{\mathbf{n}}_1\mathbf{P}_{1,0}\mathbf{y}_1 + \mathbf{n}_1^{\mathrm{T}}\mathbf{R}_1^{\mathrm{T}}\mathbf{R}_2\tilde{\mathbf{n}}_2\mathbf{P}_{2,0}\mathbf{y}_2 - \mathbf{n}_1^{\mathrm{T}}\mathbf{R}_1^{\mathrm{T}}\mathbf{R}_2\mathbf{n}_2 + (\mathbf{P}_{1,0}\mathbf{y}_1)^{\mathrm{T}}\tilde{\mathbf{n}}_1\mathbf{R}_1^{\mathrm{T}}\mathbf{R}_2\tilde{\mathbf{n}}_2\mathbf{P}_{2,0}\mathbf{y}_2\\ &= \mathbf{B}_{r,1}\mathbf{y}_1 + \mathbf{B}_{r,2}\mathbf{y}_2 - \mathrm{b} = 0\end{aligned} \tag{19}$$

$$\mathbf{B}_{r,1} = \mathbf{n}_2^{\mathrm{T}}\mathbf{R}_2^{\mathrm{T}}\mathbf{R}_1\tilde{\mathbf{n}}_1\mathbf{P}_{1,0}, \quad \mathbf{B}_{r,2} = \mathbf{n}_1^{\mathrm{T}}\mathbf{R}_1^{\mathrm{T}}\mathbf{R}_2\tilde{\mathbf{n}}_2\mathbf{P}_{2,0}, \quad \mathrm{b} = \mathbf{n}_1^{\mathrm{T}}\mathbf{R}_1^{\mathrm{T}}\mathbf{R}_2\mathbf{n}_2 - (\mathbf{P}_{1,0}\mathbf{y}_1)^{\mathrm{T}}\tilde{\mathbf{n}}_1\mathbf{R}_1^{\mathrm{T}}\mathbf{R}_2\tilde{\mathbf{n}}_2\mathbf{P}_{2,0}\mathbf{y}_2, \tag{20}$$

The rotations are determined by $\boldsymbol{\varphi}_{i,0} = \mathbf{P}_{i,0}\mathbf{y}_i$, where $\mathbf{P}_i(\mathbf{s}_i)$ represents the compatible rotations derived from the shape functions. Hereby, both Eqs. (16) and (19) become linear in $\mathbf{y}_i$ but iterations are necessary due to the rotational constraints. This can be seen in b in Eq. (20), where it is necessary to insert predicted values of $\mathbf{y}_1$ and $\mathbf{y}_2$ until it has converged.

Next, the global equations of motion are formulated by combining the equation of motion Eq. (13) for each substructure with the kinematical constraints Eqs. (16) and (19). For ease this is only demonstrated for a multibody system consisting of two substructures where the equations attain the form

$$\begin{aligned}&\begin{bmatrix}\mathbf{M}_1 & \mathbf{0} & \mathbf{0}\\ \mathbf{0} & \mathbf{M}_2 & \mathbf{0}\\ \mathbf{0} & \mathbf{0} & \mathbf{0}\end{bmatrix}\begin{bmatrix}\ddot{\mathbf{y}}_1\\ \ddot{\mathbf{y}}_2\\ \ddot{\bar{\boldsymbol{\lambda}}}\end{bmatrix} + \begin{bmatrix}\mathbf{C}_1 & \mathbf{0} & \mathbf{0}\\ \mathbf{0} & \mathbf{C}_2 & \mathbf{0}\\ \mathbf{0} & \mathbf{0} & \mathbf{0}\end{bmatrix}\begin{bmatrix}\dot{\mathbf{y}}_1\\ \dot{\mathbf{y}}_2\\ \dot{\bar{\boldsymbol{\lambda}}}\end{bmatrix} + \begin{bmatrix}\mathbf{K}_1 & \mathbf{0} & \mathbf{B}_1^{\mathrm{T}}\\ \mathbf{0} & \mathbf{K}_2 & \mathbf{B}_2^{\mathrm{T}}\\ \mathbf{B}_1 & \mathbf{B}_2 & \mathbf{0}\end{bmatrix}\begin{bmatrix}\mathbf{y}_1\\ \mathbf{y}_2\\ \bar{\boldsymbol{\lambda}}\end{bmatrix} = \begin{bmatrix}\mathbf{f}_1\\ \mathbf{f}_2\\ \mathbf{b}\end{bmatrix}\\ &\Rightarrow \mathbf{M}\ddot{\mathbf{z}} + \mathbf{C}\dot{\mathbf{z}} + \mathbf{K}\mathbf{z} = \mathbf{f}(t)\end{aligned} \tag{21}$$

where $\bar{\boldsymbol{\lambda}} = \bar{\boldsymbol{\lambda}}_1 = -\bar{\boldsymbol{\lambda}}_2$. Because the constraints in principle introduce infinite stiffness into the global system it becomes necessary to apply unconditional stable time integrators. In the present case this is achieved by means of a nonlinear Newmark algorithm.

3. System reduction

The following reduction scheme deals with a specific substructure for which reason the index i is omitted for ease. Hereby, the equations of motion for the substructure equation (13) are rewritten in the form

$$\mathbf{M}\ddot{\mathbf{y}} + \mathbf{C}\dot{\mathbf{y}} + \mathbf{K}\mathbf{y} = \mathbf{g}(t) = \mathbf{f}(t) - \mathbf{B}^{\mathrm{T}}\bar{\boldsymbol{\lambda}} \tag{22}$$

$\mathbf{g}(t)$ is a combined load vector encompassing wind loads, inertial loads, and reaction forces from the kinematical constraints.

3.1. System reduction by use of fixed–fixed and fixed–free eigenmodes

At first, the vector $\mathbf{y}$ of dimension n is partitioned into boundary $\mathbf{y}_b$ and interior $\mathbf{y}_e$ degrees of freedom i.e. $\mathbf{y}^{\mathrm{T}} = [\mathbf{y}_b^{\mathrm{T}}\ \mathbf{y}_e^{\mathrm{T}}]$. The dimensions of $\mathbf{y}_b$ and $\mathbf{y}_e$ are n_b and $n_e = n - n_b$, respectively. The method will be illustrated with beam elements with 6 degrees of freedom for each node. Hereby n_b takes either the value 6 or 12 depending on the substructure has a free end or not. The two different sets of boundary conditions are sketched in Figs. 2a and b. When a blade is modelled by two or more substructures the boundary conditions in Figs. 2a and b are used for the innermost and outermost substructures, respectively. In Figs. 2c and d constraint modes from a unit displacement for the two types of boundary conditions are sketched. Similarly, in Figs. 2e and f constraint modes from a unit rotation are sketched. Obviously, the constraint modes account for the rigid-body motion of the substructure. Eq. (22) takes the following form by use of the partitioning of $\mathbf{y}$:

$$\begin{bmatrix}\mathbf{M}_{bb} & \mathbf{M}_{be}\\ \mathbf{M}_{eb} & \mathbf{M}_{ee}\end{bmatrix}\begin{bmatrix}\ddot{\mathbf{y}}_b\\ \ddot{\mathbf{y}}_e\end{bmatrix} + \begin{bmatrix}\mathbf{C}_{bb} & \mathbf{C}_{be}\\ \mathbf{C}_{eb} & \mathbf{C}_{ee}\end{bmatrix}\begin{bmatrix}\dot{\mathbf{y}}_b\\ \dot{\mathbf{y}}_e\end{bmatrix} + \begin{bmatrix}\mathbf{K}_{bb} & \mathbf{K}_{be}\\ \mathbf{K}_{eb} & \mathbf{K}_{ee}\end{bmatrix}\begin{bmatrix}\mathbf{y}_b\\ \mathbf{y}_e\end{bmatrix} = \begin{bmatrix}\mathbf{g}_b\\ \mathbf{g}_e\end{bmatrix} \tag{23}$$

Next, the interior degrees of freedom $\mathbf{y}_e$ are written as a combination of the quasi-static response from the boundary degrees of freedom $\mathbf{y}_b$ superposed with a modal representation of the remaining part of the internal response as follows:

$$\mathbf{y}_e = -\mathbf{K}_{ee}^{-1}\mathbf{K}_{eb}\mathbf{y}_b + \boldsymbol{\Phi}\mathbf{q} \tag{24}$$

$$\mathbf{q} = \begin{bmatrix}q_1(t)\\ \vdots\\ q_{n_e}(t)\end{bmatrix}, \quad \boldsymbol{\Phi} = [\boldsymbol{\Phi}_1\ \cdots\ \boldsymbol{\Phi}_{n_e}] \tag{25}$$

$\boldsymbol{\Phi}_j$ is the jth fixed interface normal mode and q_j is the related generalized coordinate. In Figs. 2g and h an example of a fixed interface normal mode is sketched by use of the two types of boundary conditions. These eigenmodes are determined from the following generalized eigenvalue problem

$$(\mathbf{K}_{ee}(\boldsymbol{\omega}, \boldsymbol{\alpha}, \Omega) - \omega_j^2\mathbf{M}_{ee})\boldsymbol{\Phi}_j = \mathbf{0} \tag{26}$$

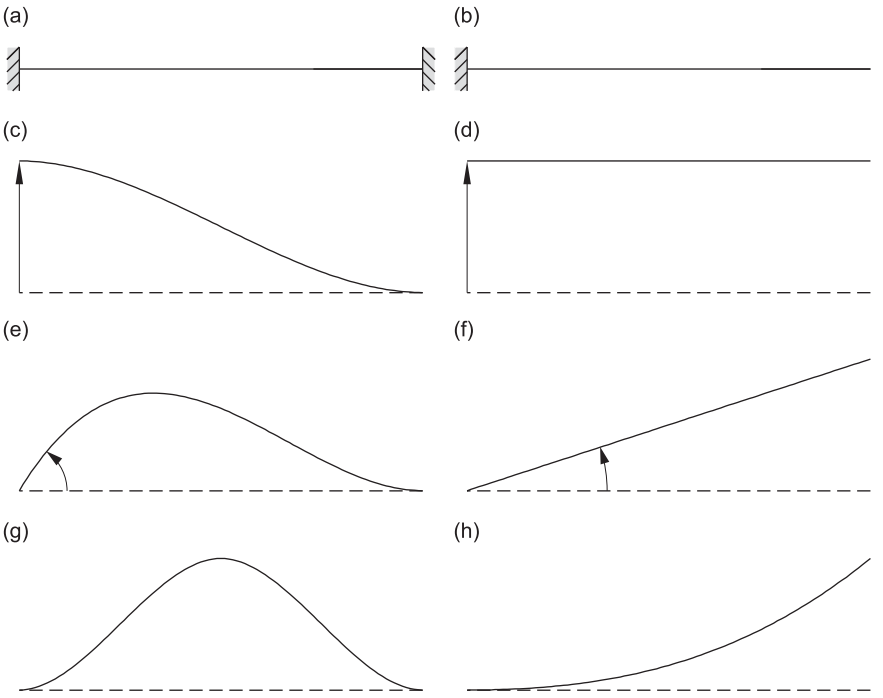

Fig. 2. (a) Boundary conditions for interior substructures. (b) Boundary conditions for substructure with a free end. (c)–(f) Constraint modes based on a unit displacement and unit rotation of the interface nodes. (g)–(h) Fixed interface normal modes.

It is intended that the eigenmodes are constant in time, whereby it is necessary to select the components of the angular velocity vector, angular acceleration vector, and the operating angular frequency, which all are used to set up the stiffness matrix in Eq. (14). ω_j denotes the undamped angular eigenfrequencies of the substructure with fixed boundary degrees of freedom $\mathbf{y}_b = \mathbf{0}$. The eigenmodes are ordered in ascending magnitude of the frequency ω_j and those with frequencies above a certain threshold frequency ω_0 are truncated, whereas the remaining eigenmodes respond dynamically. Then, the dynamic degrees of freedom $\mathbf{q}_d$ and dynamic eigenmodes $\mathbf{\Phi}_d$ become

$$\mathbf{q}_d = \begin{bmatrix} q_1(t) \\ \vdots \\ q_{n_d}(t) \end{bmatrix}, \quad \mathbf{\Phi}_d = [\mathbf{\Phi}_1 \ \cdots \ \mathbf{\Phi}_{n_d}] \tag{27}$$

where $\mathbf{q}_d$ has the dimensions $n_d < n_e$. The degrees of freedom $\mathbf{y}(t)$ and their time derivatives defining the substructure can hereby be presented in the following reduced form:

$$\mathbf{y}(t) = \mathbf{A}\mathbf{w}(t), \quad \dot{\mathbf{y}}(t) = \mathbf{A}\dot{\mathbf{w}}(t), \quad \ddot{\mathbf{y}}(t) = \mathbf{A}\ddot{\mathbf{w}}(t) \tag{28}$$

where

$$\mathbf{A} = \begin{bmatrix} \mathbf{I} & \mathbf{0} \\ \mathbf{V} & \mathbf{\Phi}_d \end{bmatrix}, \quad \mathbf{V} = -\mathbf{K}_{ee}^{-1}\mathbf{K}_{eb}, \quad \mathbf{w} = \begin{bmatrix} \mathbf{y}_b \\ \mathbf{q}_d \end{bmatrix} \tag{29}$$

Insertion of Eq. (28) in Eq. (22) and premultiplication with $\mathbf{A}^{\mathrm{T}}$ provide the following reduced equations of motion:

$$\mathbf{m}\ddot{\mathbf{w}} + \mathbf{c}\dot{\mathbf{w}} + \mathbf{k}\mathbf{w} = \mathbf{A}^{\mathrm{T}}\mathbf{g}(t) \tag{30}$$

where

$$\left.\begin{aligned} \mathbf{m} &= \mathbf{A}^{\mathrm{T}}\mathbf{M}\mathbf{A} \\ \mathbf{c} &= \mathbf{A}^{\mathrm{T}}\mathbf{C}\mathbf{A} \\ \mathbf{k} &= \mathbf{A}^{\mathrm{T}}\mathbf{K}\mathbf{A} \end{aligned}\right\} \tag{31}$$

Notice that none of the reduced matrices have a diagonal structure. To set up the system equations of motion it is necessary to partition $\mathbf{B}^{\mathrm{T}}$ and $\mathbf{f}$ in Eq. (22) consistently with the partition of $\mathbf{y}$.

3.2. System reduction by use of fixed–free eigenmodes

To be used for later comparison an alternative variant is used to model the innermost substructures of the blade. This is done by use of the procedure described above for the outermost substructure. Hereby, the innermost substructures are described by use of fixed–free eigenmodes and the dimension of the boundary degrees of freedom is $n_b = 6$ corresponding to the fixed end. Hereby, the first six columns in $\mathbf{A}$ correspond to rigid-body modes.

3.3. Reduced system of equations

Based on the derived system reduction algorithm a substructure in the system can be reduced by use of Eq. (30) together with Eq. (28) for the constraints. For the illustrative example described by Eq. (21) substructure 1 will be reduced, whereas substructure 2 is left unchanged

$$\begin{bmatrix} \mathbf{m}_1 & \mathbf{0} & \mathbf{0} \\ \mathbf{0} & \mathbf{M}_2 & \mathbf{0} \\ \mathbf{0} & \mathbf{0} & \mathbf{0} \end{bmatrix} \begin{bmatrix} \ddot{\mathbf{w}}_1 \\ \ddot{\mathbf{y}}_2 \\ \ddot{\bar{\boldsymbol{\lambda}}} \end{bmatrix} + \begin{bmatrix} \mathbf{c}_1 & \mathbf{0} & \mathbf{0} \\ \mathbf{0} & \mathbf{C}_2 & \mathbf{0} \\ \mathbf{0} & \mathbf{0} & \mathbf{0} \end{bmatrix} \begin{bmatrix} \dot{\mathbf{w}}_1 \\ \dot{\mathbf{y}}_2 \\ \dot{\bar{\boldsymbol{\lambda}}} \end{bmatrix} + \begin{bmatrix} \mathbf{k}_1 & \mathbf{0} & \mathbf{A}_1^{\mathrm{T}}\mathbf{B}_1^{\mathrm{T}} \\ \mathbf{0} & \mathbf{K}_2 & \mathbf{B}_2^{\mathrm{T}} \\ \mathbf{B}_1\mathbf{A}_1 & \mathbf{B}_2 & \mathbf{0} \end{bmatrix} \begin{bmatrix} \mathbf{w}_1 \\ \mathbf{y}_2 \\ \bar{\boldsymbol{\lambda}} \end{bmatrix} = \begin{bmatrix} \mathbf{A}_1^{\mathrm{T}}\mathbf{f}_1 \\ \mathbf{f}_2 \\ \mathbf{b} \end{bmatrix} \tag{32}$$

The state vector related to the reduced system is now defined as

$$\mathbf{z}(t) = \begin{bmatrix} \mathbf{w}_1 \\ \mathbf{y}_2 \\ \boldsymbol{\lambda} \end{bmatrix} \tag{33}$$

4. Updating of system state vector and moving frame of reference

At first an introductory overview of the following updating algorithm will be given based on a number of 2D illustrations depicted in Fig. 3. The updating scheme of the moving frame of reference follows the same principles as described in Kawamoto et al. [8]. The orientation of the moving frame of reference with the related rotation tensor $\mathbf{R}(t)$ has been indicated at various levels of the updating procedure. The corresponding degrees of freedom vector $\mathbf{y}(t)$ is symbolically indicated by the position vector of the interface node, describing the position and rotation of the substructure from the moving frame, see Fig. 3a. At the time $t = t_j$ the system state vector $\mathbf{z}_j = \mathbf{z}(t_j)$ along with its time derivatives $\dot{\mathbf{z}}_j = \dot{\mathbf{z}}(t_j)$ and $\ddot{\mathbf{z}}_j = \ddot{\mathbf{z}}(t_j)$ are known. Additionally, several parameters describing the motion of the moving frame of reference for each substructure are known. These are the global components of the position vector of the origin $\bar{\mathbf{x}}_{c,j} = \bar{\mathbf{x}}_c(t_j)$, the related velocity vector $\bar{\mathbf{v}}_{c,j} = \bar{\mathbf{v}}_c(t_j)$, and acceleration vector $\bar{\mathbf{a}}_{c,j} = \bar{\mathbf{a}}_c(t_j)$, as well as the components of the rotation tensor $\mathbf{R}_j = \mathbf{R}(t_j)$ and the moving frame components of the angular velocity and angular acceleration vectors $\boldsymbol{\omega}_j = \boldsymbol{\omega}(t_j)$, and $\boldsymbol{\alpha}_j = \boldsymbol{\alpha}(t_j)$, respectively. All these known parameters and system vectors make the starting point at the determination of the

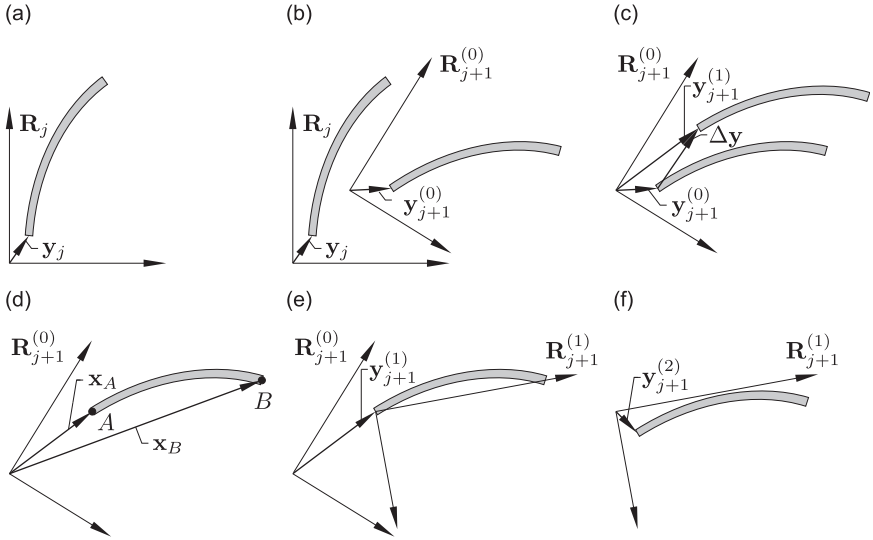

Fig. 3. (a) Moving frame and substructure at the initial situation at time $t = t_j$. (b) Prediction of moving frame and system state vector at time $t_{j+1} = t_j + \Delta t$. (c) Determination of the system state vector for the first iteration step. (d) Updating of the moving frame based on the motion of two boundary nodes. (e) Updated position and orientation of the moving frame. (f) Determination of the system state vector for the second iteration referring the motion of the substructure to the updated moving frame of reference.

corresponding quantities at the new time $t_{j+1} = t_j + \Delta t$, on condition that the new load vector $\mathbf{f}_{j+1} = \mathbf{f}(t_{j+1})$ can be calculated. In what follows an upper index (k) is used to specify the iteration step during the considered time step. Initially, predicted values based on simple Taylor expansions for the vectors related to the moving frame and the moving substructure at the time t_{j+1} are determined from the corresponding values at time t_j. Predicted values are denoted with an upper index $k = 0$, and the prediction step has been sketched in Fig. 3b. Next, the equations of motion Eq. (32) are solved with the predicted values entering the system matrices and vectors. Hereby, the nodal displacement vector for the first iteration $\mathbf{y}_{j+1}^{(1)}$ together with its time derivatives are determined, see Fig. 3c. $\Delta\mathbf{y}$ indicates the displacement difference between predicted and corrected estimates, which should be zero when the displacements of the substructure from the moving frame are converged. Based on the displacements of the substructure from the moving frame of reference another convergency criterion is set up. If these displacements are above a chosen tolerance the moving frame of reference is updated. The position of the origin together with its time derivatives is updated based on the motion of the belonging boundary node of the substructure. The orientation together with angular velocity and angular acceleration is updated by use of the motion of two boundary nodes, as sketched in Fig. 1c. In Fig. 3d both nodes are sketched, where they have been labelled A and B and the position vector in Eq. (1) from the origin of the moving frame to these nodes is denoted $\mathbf{x}_A$ and $\mathbf{x}_B$, respectively. In Fig. 3e the updated position and orientation of the moving frame of reference are illustrated. If convergence has not been achieved the updated system equations are solved again with updated system matrices and vectors. Hereby, a new nodal displacement vector $\mathbf{y}_{j+1}^{(2)}$ is determined referring the motion of the substructure to the updated moving frame of reference given by the rotation tensor $\mathbf{R}_{j+1}^{(1)}$, see Fig. 3f. This iteration continues until convergency is obtained.

Next, the indicated updating algorithm is described in a formal way. At the instant of time $t = t_{j+1}$ the vectors related to the origin of the moving frame of reference are predicted by the truncated Taylor expansions of the solution from the previous time step

$$\bar{\mathbf{x}}_{cj+1}^{(0)} = \bar{\mathbf{x}}_{cj} + \bar{\mathbf{v}}_{cj}\Delta t + \tfrac{1}{2}\bar{\mathbf{a}}_{cj}\Delta t^2, \quad \bar{\mathbf{v}}_{cj+1}^{(0)} = \bar{\mathbf{v}}_{cj} + \bar{\mathbf{a}}_{cj}\Delta t, \quad \bar{\mathbf{a}}_{cj+1}^{(0)} = \bar{\mathbf{a}}_{cj} \tag{34}$$

$\bar{\mathbf{x}}_{cj+1}^{(0)}$ is used in the displacement constraints Eq. (16). The moving frame components of the vectors defining the rotation of the moving frame of reference are similarly predicted by the Taylor expansions

$$\Delta\boldsymbol{\psi}_{j+1}^{(0)} = \boldsymbol{\omega}_j\Delta t + \tfrac{1}{2}\boldsymbol{\alpha}_j\Delta t^2, \quad \boldsymbol{\omega}_{j+1}^{(0)} = \boldsymbol{\omega}_j + \boldsymbol{\alpha}_j\Delta t, \quad \boldsymbol{\alpha}_{j+1}^{(0)} = \boldsymbol{\alpha}_j \tag{35}$$

$\Delta\boldsymbol{\psi}_{j+1}^{(0)}$ denotes the moving frame components of the predicted rotation vector of the moving frame during the interval Δt. The rotation tensor $\mathbf{R}_{j+1}^{(0)}$, corresponding to the moving frame orientation after the rotation $\Delta\boldsymbol{\psi}_{j+1}^{(0)}$, is next determined by use of Rodriguez formula Eq. (3)

$$\mathbf{R}_{j+1}^{(0)} = \mathbf{R}_j\mathbf{R}(\Delta\boldsymbol{\psi}_{j+1}^{(0)}) \tag{36}$$

In Eq. (15) the moving frame components of the acceleration of the origin are needed. These are determined from the corresponding global components via the transformation

$$\mathbf{a}_{cj+1}^{(0)} = \mathbf{R}_{j+1}^{(0)T}\bar{\mathbf{a}}_{cj+1}^{(0)} \tag{37}$$

Next, the system coordinates are predicted based on the truncated Taylor expansions

$$\mathbf{z}_{j+1}^{(0)} = \mathbf{z}_j + \dot{\mathbf{z}}_j\Delta t + \tfrac{1}{2}\ddot{\mathbf{z}}_j\Delta t^2, \quad \dot{\mathbf{z}}_{j+1}^{(0)} = \dot{\mathbf{z}}_j + \ddot{\mathbf{z}}_j\Delta t, \quad \ddot{\mathbf{z}}_{j+1}^{(0)} = \ddot{\mathbf{z}}_j \tag{38}$$

Hereby, all predicted parameters for the moving frame of reference together with the predicted system coordinates are determined. The damping matrix $\mathbf{C}^{(0)}$, stiffness matrix $\mathbf{K}^{(0)}$, and mass matrix $\mathbf{M}$ from Eq. (32) are determined next. Here, it should be noted that the mass matrix is independent of the moving frame parameters and thereby constant. In order to solve Eq. (32) the residual $\mathbf{r}$ and equivalent system stiffness matrix $\hat{\mathbf{K}}$ are determined by use of the nonlinear Newmark algorithm, Géradin and Rixen [27]

$$\mathbf{r} = -\mathbf{M}\ddot{\mathbf{z}}_{j+1}^{(0)} - \mathbf{C}^{(0)}\dot{\mathbf{z}}_{j+1}^{(0)} - \mathbf{K}^{(0)}\mathbf{z}_{j+1}^{(0)} + \mathbf{f}_{j+1}^{(0)}, \quad \hat{\mathbf{K}} = \frac{1}{\beta\Delta t^2}\mathbf{M} + \frac{\gamma}{\beta\Delta t}\mathbf{C}^{(0)} + \mathbf{K}^{(0)} \tag{39}$$

where $\gamma = \frac{1}{2} + \alpha$, $\beta = \frac{1}{4}(1+\alpha)^2$, and α is used to incorporate numerical damping. By solving $\hat{\mathbf{K}}\Delta\mathbf{z} = \mathbf{r}$ for the unknowns $\Delta\mathbf{z}$, the following corrected values of the system coordinates are determined:

$$\mathbf{z}_{j+1}^{(1)} = \mathbf{z}_{j+1}^{(0)} + \Delta\mathbf{z}, \quad \dot{\mathbf{z}}_{j+1}^{(1)} = \dot{\mathbf{z}}_{j+1}^{(0)} + \frac{\gamma}{\beta\Delta t}\Delta\mathbf{z}, \quad \ddot{\mathbf{z}}_{j+1}^{(1)} = \ddot{\mathbf{z}}_{j+1}^{(0)} + \frac{1}{\beta\Delta t^2}\Delta\mathbf{z} \tag{40}$$

Hereby the displacement and rotation degrees of freedom of the substructure referred to the moving frame of reference can be determined together with their time derivatives. In case of using the reduced models the transformations to the full set of degrees of freedom are performed by use of Eq. (28). The displacements and rotations at the boundaries are referred to as $\mathbf{u}_A$, $\boldsymbol{\varphi}_A$, and $\mathbf{u}_B$, $\boldsymbol{\varphi}_B$. The same notation follows for the time derivatives of the displacements and rotations. The used convergency criterion is based on the position of the moving frame of reference. Therefore, the Euclidian norms of $\mathbf{u}_A$ and $\mathbf{u}_B$ are used. If these norms are within a chosen tolerance there is no need to update the moving frame of reference and the

present solution is used as input in the new time step. If this is not the case, the moving frame of reference parameters are updated.

The position, velocity and acceleration of the origin of the moving frame of reference are updated by use of Eqs. (2), (5) and (6)

$$\bar{\mathbf{x}}_{c,j+1}^{(k+1)} = \bar{\mathbf{x}}_{c,j+1}^{(k)} + \mathbf{R}_{j+1}^{(k)}\mathbf{u}_A \tag{41}$$

$$\bar{\mathbf{v}}_{c,j+1}^{(k+1)} = \bar{\mathbf{v}}_{c,j+1}^{(k)} + \mathbf{R}_{j+1}^{(k)}(\tilde{\boldsymbol{\omega}}_{j+1}^{(k)}(\mathbf{s}+\mathbf{u}_A) + \dot{\mathbf{u}}_A) \tag{42}$$

$$\bar{\mathbf{a}}_{c,j+1}^{(k+1)} = \bar{\mathbf{a}}_{c,j+1}^{(k)} + \mathbf{R}_{j+1}^{(k)}((\tilde{\boldsymbol{\alpha}}_{j+1}^{(k)} + \tilde{\boldsymbol{\omega}}_{j+1}^{(k)}\tilde{\boldsymbol{\omega}}_{j+1}^{(k)})(\mathbf{s}+\mathbf{u}_A) + 2\tilde{\boldsymbol{\omega}}_{j+1}^{(k)}\dot{\mathbf{u}}_A + \ddot{\mathbf{u}}_A) \tag{43}$$

In the following, the update of the orientation, angular velocity and angular acceleration of the moving frame of reference is described, which is based on the motion of both boundary nodes A and B. The purpose of the present update is to align the beam axis and thereby the x_3-axis so it passes through both nodes. In order to determine the orientation of the remaining x_1- and x_2-axes the average rotation φ_3 around the beam axis is used, which is given by the third rotation component at the two nodes

$$\varphi_3 = \tfrac{1}{2}(\varphi_{B,3} + \varphi_{A,3}) \tag{44}$$

Then, the two basis vectors $\mathbf{n}_1$ and $\mathbf{n}_2$ for the x_1- and x_2-axis are given as

$$[\mathbf{n}_1\ \mathbf{n}_2\ \mathbf{n}_3] = \begin{bmatrix} \cos\varphi_3 & -\sin\varphi_3 & 0 \\ \sin\varphi_3 & \cos\varphi_3 & 0 \\ 0 & 0 & 1 \end{bmatrix} \tag{45}$$

The purpose is to rotate the full basis through the minimum angle bringing one of the vectors into a given new direction. In the present case the vector $\mathbf{n}_3$ is to be rotated into the direction of the beam axis defined by the unit vector $(\mathbf{x}_B - \mathbf{x}_A)/|\mathbf{x}_B - \mathbf{x}_A|$, where $\mathbf{x}_A$ and $\mathbf{x}_B$ are the position vectors of the end nodes relative to the moving frame origin cf. Fig. 3d. First, the mean direction is defined by the unit vector $\mathbf{n}$

$$\mathbf{n} = \mathbf{n}_3 + \frac{\mathbf{x}_B - \mathbf{x}_A}{|\mathbf{x}_B - \mathbf{x}_A|}, \quad \mathbf{n} := \mathbf{n}/|\mathbf{n}| \tag{46}$$

Next, a Householder transformation is used, which corresponds to a reflection in the plane orthogonal to the unit vector $\mathbf{n}$, Krenk [28]

$$\Delta\mathbf{R} = (\mathbf{I} - 2\mathbf{n}\mathbf{n}^{\mathrm{T}})[\mathbf{n}_1\ \ \mathbf{n}_2\ \ -\mathbf{n}_3] \tag{47}$$

Hereby, a new set of unit vectors contained in $\Delta\mathbf{R}$ are determined, which describe the updated orientation seen from the present orientation of the moving frame of reference. The updated rotation tensor is given by, cf. Fig. 3e

$$\mathbf{R}_{j+1}^{(k+1)} = \mathbf{R}_{j+1}^{(k)}\Delta\mathbf{R} \tag{48}$$

In order to update the angular velocity it is used that the global components of the velocity at node B should be the same in the present known configuration of the moving frame and in the updated one. The global components of the velocity at node B are determined by use of Eq. (5)

$$\bar{\mathbf{v}}_B = \bar{\mathbf{v}}_{c,j+1}^{(k)} + \mathbf{R}_{j+1}^{(k)}(\tilde{\boldsymbol{\omega}}_{j+1}^{(k)}(\mathbf{s}_B + \mathbf{u}_B) + \dot{\mathbf{u}}_B) \tag{49}$$

where $\mathbf{s}_B$ given in the updated moving frame of reference marks the node B. The updating strategy presumes that the local displacement and velocity at B vanish, cf. Fig. 3e. Hereby, by use of Eq. (5) and the results from Eq. (49) the following relation is obtained for the updated angular velocity

$$\mathbf{R}_{j+1}^{(k+1)^{\mathrm{T}}}(\bar{\mathbf{v}}_B - \bar{\mathbf{v}}_{c,j+1}^{(k+1)}) = \tilde{\boldsymbol{\omega}}_{j+1}^{(k+1)}\mathbf{s}_B \tag{50}$$

The two first rows give a solution for the two first components of the angular velocity $\omega_{1,j+1}^{(k+1)}$ and $\omega_{2,j+1}^{(k+1)}$. The third component is determined from the previous known value and the average of the belonging angular velocity component of the two nodes

$$\omega_{3,j+1}^{(k+1)} = \omega_{3,j+1}^{(k)} + \tfrac{1}{2}(\dot{\varphi}_{B,3} + \dot{\varphi}_{A,3}) \tag{51}$$

Similarly, the angular acceleration is determined by use of Eq. (6)

$$\bar{\mathbf{a}}_B = \bar{\mathbf{a}}_{c,j+1}^{(k)} + \mathbf{R}_{j+1}^{(k)}((\tilde{\boldsymbol{\alpha}}_{j+1}^{(k)} + \tilde{\boldsymbol{\omega}}_{j+1}^{(k)}\tilde{\boldsymbol{\omega}}_{j+1}^{(k)})(\mathbf{s}_B + \mathbf{u}_B) + 2\tilde{\boldsymbol{\omega}}_{j+1}^{(k)}\dot{\mathbf{u}}_B + \ddot{\mathbf{u}}_B) \tag{52}$$

$$\mathbf{R}_{j+1}^{(k+1)^{\mathrm{T}}}(\bar{\mathbf{a}}_B - \bar{\mathbf{a}}_{c,j+1}^{(k+1)}) - \tilde{\boldsymbol{\omega}}_{j+1}^{(k+1)}\tilde{\boldsymbol{\omega}}_{j+1}^{(k+1)}\mathbf{s}_B = \tilde{\boldsymbol{\alpha}}_{j+1}^{(k+1)}\mathbf{s}_B \tag{53}$$

$$\alpha_{3,j+1}^{(k+1)} = \alpha_{3,j+1}^{(k)} + \tfrac{1}{2}(\ddot{\varphi}_{B,3} + \ddot{\varphi}_{A,3}) \tag{54}$$

5. Numerical example

In this section the theory is illustrated with a simplified system consisting of a wind turbine blade divided into two substructures labelled 1 and 2. The fixed frame of reference is shown in Fig. 4a and the two substructures are shown in Fig. 4b. The origin of the initial moving frame of reference $(x_{1,1}, x_{2,1}, x_{3,1})$ belonging to substructure 1 is identical to the fixed frame of reference $(\bar{x}_1, \bar{x}_2, \bar{x}_3)$ whereas the origin of the initial moving frame of reference $(x_{1,2}, x_{2,2}, x_{3,2})$ belonging to substructure 2 is displaced half the blade length in the $\bar{x}_3$-direction. In total 11 constraints are introduced where six fix displacements and rotations at the assembling point of the two substructures. The remaining five constraints are used at the origin of substructure 1. Here, three constraints fix the displacements and two constraints fix the rotation around the $\bar{x}_2$- and $\bar{x}_3$-axes. I.e. at the root it is only possible for the blade to rotate around the $\bar{x}_1$-axis. The moving frame of reference for both substructures is updated based on the motion of the two end points in each substructure. The updating algorithm is described in Section 4 and the x_3-axis for the two moving frames are sketched in Fig. 4c. The length of the blade is 44.8 m with a total weight of 10 t and it is constructed by NACA 63-418 section profiles. The cross section parameters throughout the blade are presented in Fig. 5. A Young's modulus of $E = 3 \times 10^{10}$ Pa, shear modulus of $G = E/2.6$, and density $\rho = 2 \times 10^3\ \mathrm{kg\,m^{-3}}$ are used for all sections. The element stiffness matrix is setup in principal directions and rotated the angle ϕ to align with the (x_1, x_2)-coordinate system, see Fig. 5f. The FE model of both substructures is based on prismatic Bernoulli–Euler beam elements with St. Venant torsion and has 6 degrees of freedom for each node. Both substructures have equal reference length of 22.4 m and both are discretized by use of 10 prismatic elements of equal length. This FE model constitutes the full model which the reduced models are compared to. No structural damping is included i.e. $\mathbf{C}_0 = \mathbf{0}$ in Eq. (14) and $\alpha = 0.08$ is used to incorporate numerical damping in the nonlinear Newmark algorithm with constant time steps of $\Delta t = 0.02$ s. The moving frames are updated in each time step. In Holm-Jørgensen and Nielsen [11] the three lowest undamped fixed-base circular eigenfrequencies of the blade are $\omega_1 = 5.15$, $\omega_2 = 9.51$, and $\omega_3 = 14.23$. In determining these a constant angular velocity of the moving frame corresponding to the operating frequency of the rotor is used to set up the stiffness matrix.

The purpose of the numerical simulation is to verify that the results from the reduced model based on fixed–fixed interface normal modes for substructure 1 are almost identical to the full FE model. Moreover, the importance of using compatible interface normal modes at the assembling point to substructure 2 is illustrated by use of fixed–free interface normal modes for substructure 1, with the free end at the assembling points. For both reduced models, substructure 2 is modelled by use of fixed–free interface normal modes. For comparison of the two reduced models it is chosen to keep the same number of degrees of freedom. When referring to the number of fixed–fixed and fixed–free interface normal modes, it is only the modes with the lowest eigenfrequencies cf. Eq. (26) which are used and the remaining modes are truncated. In one case substructure 1 has 12 boundary degrees of freedom and three fixed–fixed interface normal modes. In the other case substructure 1 is modelled by 6 boundary degrees of freedom and nine fixed–free interface normal modes. In both

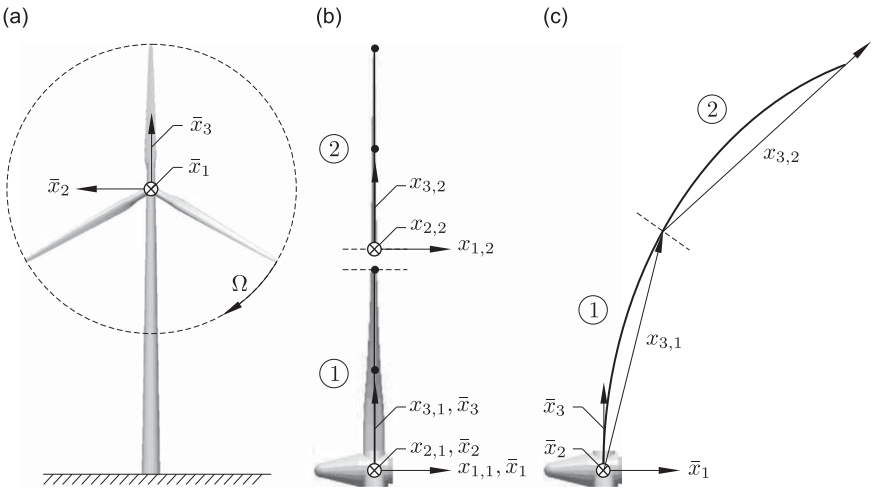

Fig. 4. (a) Fixed frame of reference in the wind turbine. (b) In the numerical model the blade is divided into two substructures labelled 1 and 2. (c) Illustration of the x_3-axis for the moving frame of reference belonging to substructure 1 and 2 denoted by $x_{3,1}$ and $x_{3,2}$, respectively.

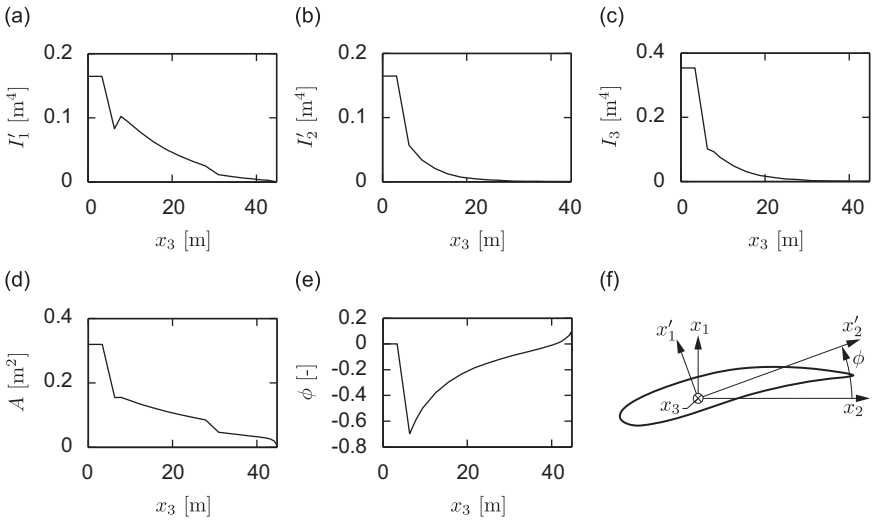

Fig. 5. (a) Principal moment of inertia around x_1'. (b) Principal moment of inertia around x_2'. (c) St. Venant torsional constant. (d) Areal of cross section. (e) Pretwist angle defined as the angle between the tangential x_2-axis and principal x_2'-axis. (f) Sign definition of ϕ.

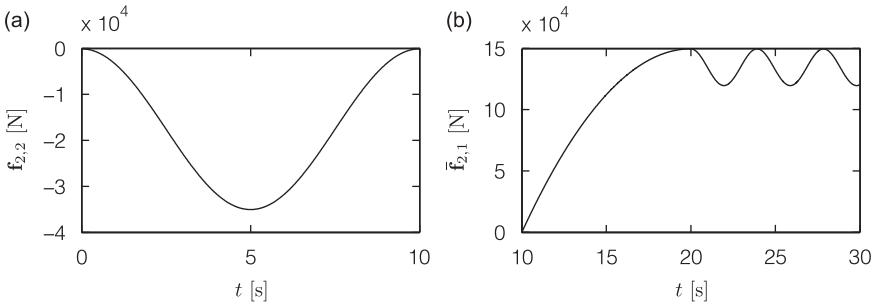

Fig. 6. (a) Load component in the x_2-direction. (b) Load component in the $\bar{x}_1$-direction.

cases substructure 2 is modelled as fixed–free with a total of 6 boundary degrees of freedom and 12 fixed–free interface normal modes. Hereby, the FE model has 132 degrees of freedom and the reduced models have 33 degrees of freedom.

5.1. Exterior load and fixed interface normal modes

The numerical simulation consists of a start-up sequence and an operating sequence. The start-up sequence is split in two where the first sequence $0 \le t \le t_1$ speeds up the blade from a stopped situation at $t = 0$ to the nominal angular velocity $\Omega_n = 1.6\,\mathrm{rads}^{-1}$ of the rotor at $t = t_1$. In the second sequence $t_1 < t \le t_2$ an exterior load in the global $\bar{x}_1$-direction is stepped up. In the operating sequence $t > t_2$ the exterior load is based on a constant load corresponding to a mean wind velocity and a harmonic component due to a variation in the shear wind field. The sequences are modelled by applying concentrated loads at a node in the beam model placed at the moving coordinate $x_{3,2} = 6.72$ m. The reason for applying the load at this point is because the maximum intensity of the wind load is concentrated around this position. The components of the applied exterior load at substructure 2 are shown in Fig. 6 and defined as

$$\mathbf{f}_2(t) = \begin{cases} [0\ 1\ 0]^{\mathrm{T}} \dfrac{1}{2} P_0 \left(1 - \cos\left(\dfrac{2\pi}{t_1} t\right)\right), & 0 \le t \le t_1 \\ \mathbf{R}_2^{\mathrm{T}} [1\ 0\ 0]^{\mathrm{T}} P_1 \left(-\left(\dfrac{t - t_1}{t_2 - t_1}\right)^2 + 2\dfrac{t - t_1}{t_2 - t_1}\right), & t_1 < t \le t_2 \\ \mathbf{R}_2^{\mathrm{T}} [1\ 0\ 0]^{\mathrm{T}} P_1 \left(1 + p\cos(\Omega_n (t - t_2)) - p\right), & t > t_2 \end{cases} \tag{55}$$

Here, it is seen that the applied load in the sequence $0 \le t \le t_1$ is oriented in the edge direction in order to speed-up the blade. In the other two sequences the load is oriented in the $\bar{x}_1$-direction i.e. primarily in the flap direction. In the simulations the following values have been used: $P_0 = -3.5 \times 10^4$ N, $P_1 = 1.5 \times 10^5$ N, $p = 0.1$, $\Omega_n = 1.6\,\mathrm{rad} - \mathrm{s}^{-1}$, $t_1 = 10$ s, and $t_2 = 20$ s. Based on the applied load the components of the angular velocity and angular acceleration of the

moving frames during the time series are determined by use of the FE model. The orientation of the moving frames given by the parameter vector $\boldsymbol{\theta}$ is determined by use of Spurriers algorithm, see e.g. Crisfield [29]. All three components of the parameter vector, angular velocity, and angular acceleration for the two moving frames are plotted in Fig. 7. Here, it is shown that for both substructures 1 and 2 the first component of the angular velocity of the belonging moving frame of reference is almost constant at $\omega_{1,1} \simeq \omega_{1,2} \simeq 1.6\,\mathrm{rad\,s^{-1}}$ in the operating sequence $t > t_2$ and considerably larger than the second and third components. The reason for not being constant is because no generator is applied to control the angular velocity. Another reason is that the blade is twisted resulting in both flap and edge wise displacements when a load in the flap direction is applied. It can also be seen that all second and third components for substructure 1 are considerably smaller than for substructure 2. This is due to the small displacement in the $\bar{x}_1$-direction at the end node of this substructure which leaves the $x_{3,1}$-axis almost orthogonal to the $\bar{x}_1$-axis. Moreover, in the operating situation the angular acceleration is close to zero. When creating the fixed interface normal modes Eq. (26) for the reduced models it is computational advantageous if these are constant throughout the simulated time series. Similarly with the constraint modes listed in Eq. (29). As seen from Eq. (14), the stiffness matrix consists of the elastic stiffness $\mathbf{K}_e$, the geometric stiffness $\mathbf{K}_g$ and the gyroscopic stiffness terms $\mathbf{D}$ and $\dot{\mathbf{G}}$ which depend on the angular velocity and angular acceleration of the moving frame, respectively. In a previous paper by the authors [11] three different stiffness matrices were used to extract the eigenmodes for a blade modelled by fixed–free eigenmodes, depending on different values of the angular velocity and angular acceleration vectors and different terms of the included stiffness matrices from Eq. (14). Small differences were observed but the overall best results were obtained by use of

$$\mathbf{K} = \mathbf{K}_e + \mathbf{K}_g(\Omega_n) + \mathbf{D}(\boldsymbol{\omega}_n), \quad \boldsymbol{\omega}_n = \begin{bmatrix} \Omega_n \\ 0 \\ 0 \end{bmatrix} \tag{56}$$

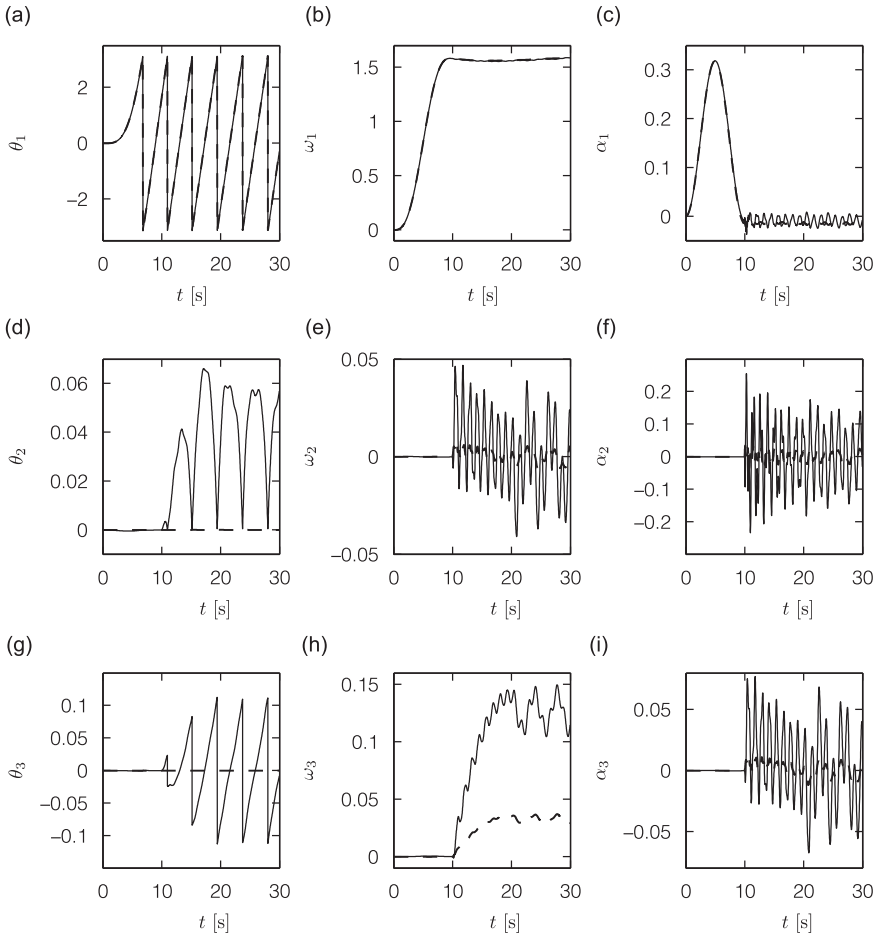

Fig. 7. Moving frame components of the parameter vector $\boldsymbol{\theta}$, angular velocity $\boldsymbol{\omega}$, and angular acceleration $\boldsymbol{\alpha}$ for the two moving frames. (a)–(c) First component. (d)–(f) Second component. (g)–(i) Third component. (- -) Substructure 1. (—) Substructure 2.

which is used for both substructures in the present simulations. For all situations the same mass matrix **M** from Eq. (10) is used when solving the generalized eigenvalue problem Eq. (26).

5.2. Results for response and constraint

Results for the tip position of the blade in $\bar{x}_1$ during the time series $10 \leq t \leq 30$ s are shown in Fig. 8a for the FE model, and the two reduced models with fixed–fixed and fixed–free interface normal modes for substructure 1. The results from the FE model are used to normalize the results from the reduced models shown in Fig. 8b. The reason for not displaying the first 10 s is because these displacements in $\bar{x}_1$ are small, and the normalized response of the reduced models is outside the area of interest. In Fig. 8b the results by use of the fixed–fixed modes are very close to the full FE model, even though these modes are constant throughout the time series. Moreover, these modes are based on a constant angular velocity around just one axis, where it is shown in Fig. 7 that this is not the actual case, especially for substructure 2. By use of the fixed–free modes the size of the response is notably changed. The importance of using compatible interface normal modes at the assembling point between the substructures is hereby demonstrated.

In Fig. 9a the Lagrange multiplier for the displacement constraint in the $\bar{x}_1$-direction at the root of the blade is shown. Here, the reaction force is approximately P_1 at $t = 20$ s and has a mean value of approximately 1.35×10^5 N for $t > 20$ s corresponding to the applied load component. In Fig. 9b the normalized Lagrange multiplier by use of fixed–fixed and fixed–free interface normal modes for substructure 1 is presented. Again, the best results are obtained by use of fixed–fixed modes, but the results by use of fixed–free modes are at least centred around the results from the FE model.

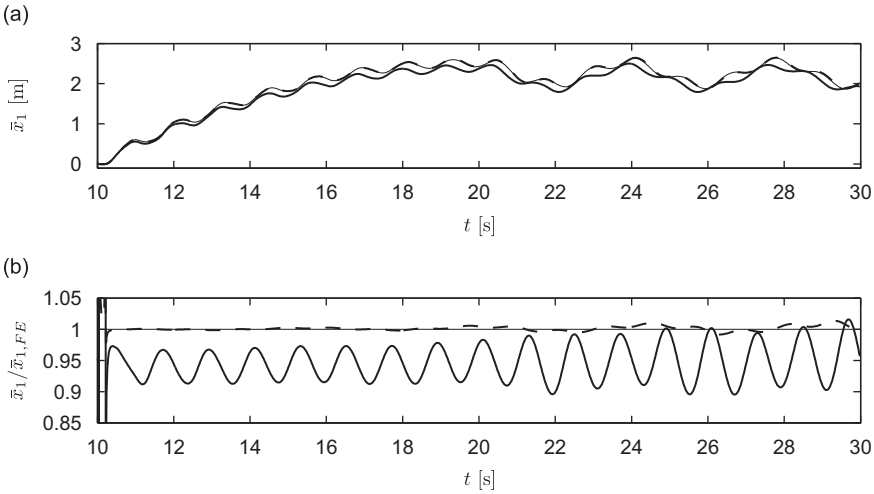

Fig. 8. (a) Tip position in $\bar{x}_1$. (b) Normalized tip position in $\bar{x}_1$. (—) FE model. (- -) Fixed–fixed modes. (—) Fixed–free modes.

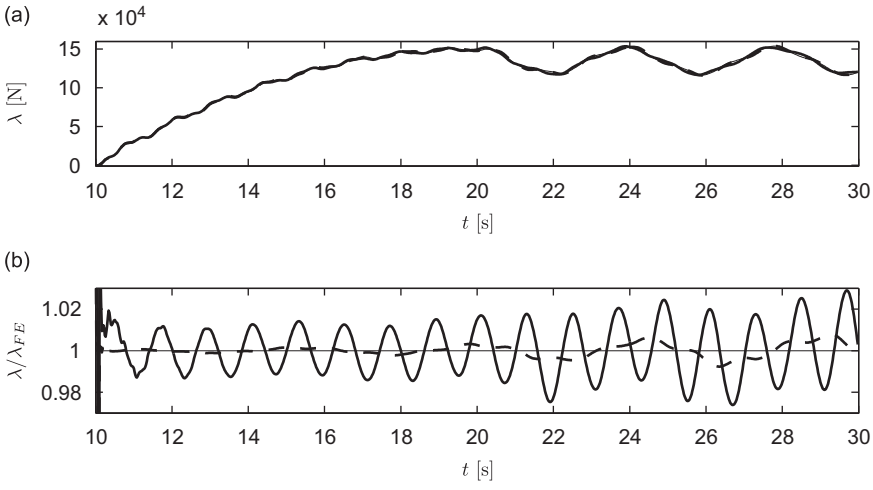

Fig. 9. (a) Lagrange multiplier for displacement constraint in the $\bar{x}_1$-direction at the hub of the blade. (b) Normalized Lagrange multiplier. (—) FE model. (- -) Fixed–fixed modes. (—) Fixed–free modes.

6. Conclusions

In this paper it is demonstrated that an FE model of a wind turbine blade divided into two substructures in the used multibody formulation with completely freely moving local frames of reference efficiently can be reduced by use of constraint modes and fixed interface normal modes. Even by keeping these modes constant throughout the numerical simulations, where the blade goes from a stopped situation to the nominal operating situation, the results are almost identical to the full FE model. The importance of using compatible modes at the assembling point between the substructures of the blade is demonstrated. Further, an updating algorithm for the freely moving frame based on the motion of two arbitrary nodes in the substructure has been devised and its applicability has been demonstrated by use of the end nodes in the belonging substructures. For smaller displacements of the substructure from the moving frame of reference and to get a better nonlinear description of the displacements the reference length of the two multibodies should be further examined instead of splitting the blade into two multibodies of equal reference length.

Acknowledgements

This work has been supported by the Danish Council for Strategic Research through the project 'Nonlinear Multibody Dynamics of Wind Turbines'.

References

[1] O.P. Agrawal, A.A. Shabana, Dynamic analysis of multibody systems using component modes, *Computers & Structures* 21 (6) (1985) 1303–1312.
[2] A.A. Shabana, Resonance conditions and deformable body co-ordinate systems, *Journal of Sound and Vibration* 192 (1) (1996) 389–398.
[3] P.E. Nikravesh, *Computer-aided Analysis of Mechanical Systems*, Prentice-Hall, Englewood Cliffs, NJ, 1988.
[4] J.G. de Jalón, E. Bayo, *Kinematic and Dynamic Simulations of Multibody Systems—The Real-Time Challenge*, Springer, Berlin, 1993.
[5] M. Géradin, A. Cardona, *Flexible Multibody Dynamics — A Finite Element Approach*, Wiley, New York, 2001.
[6] A.A. Shabana, *Dynamics of Multibody Systems*, third ed., Cambridge University Press, Cambridge, 2005.
[7] A. Kawamoto, M. Inagaki, T. Aoyama, K. Yasuda, Vibration of moving flexible bodies (formulation of dynamics by using normal modes and a local observer frame), *Proceeding of DETC99/VIB-8232*, 1999.
[8] A. Kawamoto, S. Krenk, A. Suzuki, Flexible body dynamics in a freely floating local frame, *ECCOMAS Conference on Multibody Dynamics 2007*, Milan, Italy, 25–28 June 2007.
[9] A. Kawamoto, A. Suzuki, M. Inagaki, S. Krenk, Flexible-body dynamics in a floating frame with extraction of rigid body motion, *4th Asian Conference on Multibody Dynamics 2008*, ACMD, Jeju, Korea, August 20–23, 2008.
[10] A. Kawamoto, S. Krenk, A. Suzuki, M. Inagaki, Flexible body dynamics in a local frame of reference with explicitly predicted motion, *International Journal for Numerical Methods in Engineering* 2009, to appear.
[11] K. Holm-Jorgensen, S.R.K. Nielsen, System reduction in multibody dynamics of wind turbines, *Journal of Multibody System Dynamics* 21 (2009) 147–165.
[12] R.J. Guyan, Reduction of stiffness and mass matrices, *AIAA Journal* 3 (1965) 380.
[13] K.-J. Bathe, *Finite Element Procedures*, Prentice-Hall, Englewood Cliffs, NJ, 1988.
[14] A.Y.T. Leung, An accurate method of dynamic substructuring with simplified computation, *International Journal of Numerical Methods in Engineering* 14 (1979) 1241–1256.
[15] A.Y.T. Leung, A simplified dynamic substructure method, *Earthquake Engineering and Structural Dynamics* 14 (1988) 827–837.
[16] A.Y.T. Leung, *Dynamic Stiffness and Substructures*, Springer, Berlin, 1993.
[17] N. Petersmann, Calculation of eigenvalues using substructures and dynamic condensation, *Proceedings of the 2nd International Conference on Recent Advances in Structural Dynamics 1984*, Southampton, April 1984, pp. 211–219.
[18] N. Bouhaddi, R. Fillod, Model reduction by a simplified variant of dynamic condensation, *Journal of Sound and Vibration* 191 (2) (1996) 233–250.
[19] Z.-Q. Qu, Z.-F. Fu, An iterative method for dynamic condensation of structural matrices, *Mechanical Systems and Signal Processing* 14 (4) (2000) 667–678.
[20] Z.-Q. Qu, W. Chang, Dynamic condensation method for viscously damped vibration systems in engineering, *Engineering Structures* 23 (2000) 1426–1432.
[21] Z.-Q. Qu, R.P. Selvam, Insight into the dynamic condensation technique of non-classically damped models, *Journal of Sound and Vibrations* 272 (2004) 581–606.
[22] W.C. Hurty, Dynamic analysis of structural systems using component modes, *AIAA Journal* 3 (4) (1965) 678–685.
[23] W.C. Hurty, J.D. Collins, G.C. Hart, Dynamic analysis of large structures by modal synthesis techniques, *Computers & Structures* 1 (1971) 535–563.
[24] R.R. Craig Jr., M.C.C. Bampton, Coupling of substructures for dynamic analysis, *AIAA Journal* 6 (7) (1968) 1313–1319.
[25] J.A.C. Ambrósio, J.P.C. Gonçalves, Complex flexible multibody systems with application to vehicle dynamics, *Multibody System Dynamics* 6 (2001) 163–182.
[26] A. Shanmugam, C. Padmanabhan, A fixed–free interface component mode synthesis method for rotordynamic analysis, *Journal of Sound and Vibration* 297 (2006) 664–679.
[27] M. Géradin, D. Rixen, *Mechanical Vibrations: Theory and Application to Structural Dynamics*, second ed., Wiley, New York, 1997.
[28] S. Krenk, *Non-Linear Modeling and Analysis of Solids and Structures*, Cambridge University Press, Cambridge, 2009.
[29] M.A. Crisfield, *Non-Linear Finite Element Analysis of Solids and Structures, Advanced Topics*, vol. 2, Wiley, New York, 1997.